Orbital
The electronic journal of chemistry

the electronic journal of chemistry

Full Paper | http://dx.doi.org/10.17807/orbital.v17i6.23219

Synthesis and Characterization of Novel Rhenium Tricarbonyl Complexes with Dipicolylamine Sulfonamide Ligands: Potential Serine/threonine Kinase Inhibitors for Cancer Therapy

Pamodya P. Weerasuriya [a], Kithmini Yasarathna [a], Lashan Edirisinghe [a], Frank R. Fronczek [b], Inoka C. Perera [c], and Theshini Perera* [a]

This study explores the synthesis of rhenium complexes using two novel ligands; *N*(SO_2(Iodobenz))dpa (**L1**) and *N*(SO_2(tfm)py)dpa (**L2**). The formation of these ligands and their corresponding rhenium complexes, [$Re(CO)_3$(**L1**)]$^+$ (**C1**) and [$Re(CO)_3$(**L2**)]$^+$ (**C2**), was meticulously confirmed through ^{1}H and ^{13}C NMR spectroscopic analysis. Interestingly, the singlet peak associated with the methylene hydrogens in the ligands (4.54 ppm for **L1** and 4.66 ppm for **L2**) transformed into two doublets in the complexes, indicating distinct magnetic environments upon complexation with rhenium. Structural verification via single-crystal diffraction confirmed the successful synthesis of **L1, L2, C1** and **C2.** UV-Visible spectroscopic analysis aided in the identification of π−π* transitions within the 200-265 nm range for ligands, and MLCT (metal-to-ligand charge transfer) transitions around 310 nm for the complexes. FTIR spectra exhibited significant changes in the S-N stretching bands of **L1** (916 cm^{-1}) and **L2** (919 cm^{-1}) upon coordinating to Re (**C1** (832 cm^{-1}) and **C2** (830 cm^{-1}). While both ligands displayed considerable fluorescence, both complexes showed quenched fluorescence. Swiss TargetPrediction analysis indicated the potential of these compounds as Serine/Threonine protein kinase inhibitors. Molecular docking studies of **L1**, **L2**, **C1** and **C2** with human Serine/Threonine protein kinase Aurora A and PIM2 revealed favorable binding affinities and emphasize their potential as lead compounds in the cancer drug development.

Graphical abstract

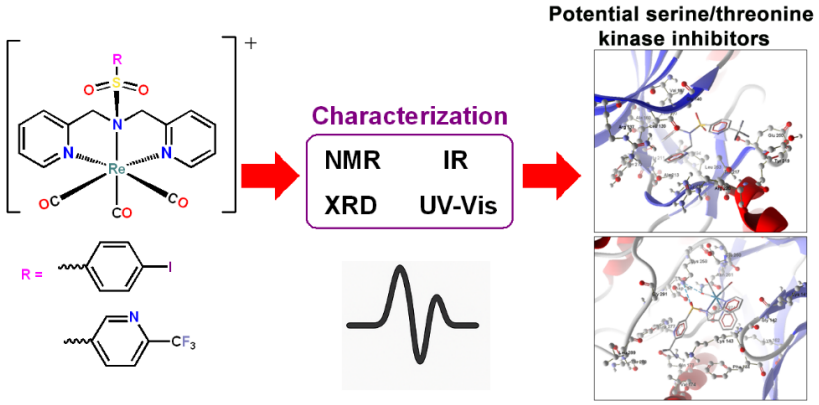

Keywords

Cancer drugs
Dipicolylamine sulfonamide ligands
Kinase inhibitors
Rhenium tricarbonyl complexes

Article history

Received 25 May 2025
Revised 24 Nov 2025
Accepted 06 Jan 2026
Available online 20 Jan 2026

Handling Editor: Vania D. Schwade

[a] Department of Chemistry, University of Sri Jayewardenepura, Nugegoda, 10250, Sri Lanka. [b] Department of Chemistry, Louisiana State University, Baton Rouge, Louisiana, 70803, USA. [c] Department of Zoology and Environment Sciences, University of Colombo, Colombo 03, Sri Lanka. *Corresponding author: Theshini Perera, Department of Chemistry, University of Sri Jayewardenepura, Nugegoda, 10250, Sri Lanka. Email: **theshi@sjp.ac.lk**

1. Introduction

Cancer is described as a group of diseases characterized by the uncontrolled growth and spread of abnormal cells in the body. These abnormal cells, known as cancer cells, can invade and destroy surrounding tissues and organs. Shockingly, recent statistics reveal that cancer is responsible for approximately one in six deaths attributed to diseases [1]. The accidental but welcome discovery of the anticancer properties of *cis*-platin by Rosenberg and co-workers [2] marked a significant turning point, igniting interest in the exploration and development of metal complexes for medicinal applications [3]. This discovery has led to exciting research bringing new insights to treat cancer using metal complexes [3, 4].

Recent investigations have unveiled the diverse potential of metal complexes as cancer treatments beyond platinum, aiming to overcome drawbacks such as acute and chronic side effects and the tendency of resistance by cancer cells [5,6]. Metals such as platinum, gold, ruthenium, iron, iridium, zinc, rhenium and copper have shown potential as cancer therapeutics [3–6]. This study centers on the synthesis of rhenium complexes, which hold promise for cancer treatment [7,8]. Rhenium boasts a spectrum of isotopes, including radioactive variants like ^{186}Re and ^{188}Re currently employed in cancer therapy [9]. Chemically similar to technetium, rhenium shares analogous properties [10] with ^{99m}Tc which is widely used as an organ imaging agent [11], and is indeed the most prevalent diagnostic radioisotope. Non-radioactive rhenium analogues serve as invaluable models for comprehending ligand design and the characteristics of radioactive ^{99m}Tc complexes. The core structure *fac*-$\{Re(CO)_3\}^+$ mirrors the role of *fac*-$\{^{99m}Tc(CO)_3\}^+$ in developing novel clinical imaging agents [12, 13].

The development of new cancer treatments includes strategies that focus on inhibiting specific molecules, like kinases, which play a crucial role in promoting tumor growth [14]. Kinases are key enzymes that are essential in regulating cellular functions such as growth, proliferation, survival, and apoptosis, all processes often dysregulated in cancer cells. When certain types of kinases, specifically serine/threonine kinases, become abnormally active, they can contribute to the initiation and advancement of cancer [15]. PIM (Proviral Integration site for Moloney murine leukemia virus) and Aurora kinase are two families of serine/threonine kinases. During leukemia and solid tumors PIM2 kinase overexpresses and promote cell survival, inhibit apoptosis, and contribute to cancer cell proliferation and growth [16,17]. Similarly, Aurora-A is also overexpressed in tumor cells and plays a vital role in tumor formation and progression by regulating mitotic processes, including centrosome maturation, spindle assembly, and chromosome segregation [18].

Aurora-A and PIM2 kinases are attractive targets for anticancer therapy due to their critical roles in promoting tumor growth, survival, and metastasis. Targeting these kinases with specific inhibitors holds promise for developing novel cancer treatments that could improve disease outcomes [19]. Although most studied inhibitors are small organic molecules [14,19,20] there are a few examples of gold, platinum, ruthenium and osmium complexes which are used as kinase inhibitors [21–24]. To the best of our knowledge, only two rhenium complexes with N-heterocyclic carbene have been reported to display potential to be used as a kinase inhibitor [25,26]. Therefore, this study would be the first study that reports the rhenium tricarbonyl complexes bearing dipicolylamine appended sulfonamide ligands as potential kinase inhibitors with anticancer properties.

Herein, we report on the potential ability of two novel rhenium dipicolylamine complexes with a sulfonamide moiety (Fig. 1) as a cancer therapeutic via enzyme inhibition. Dipicolylamine complexes of rhenium hold promise as radiopharmaceuticals [27] and imaging agents [28,29]. Additionally, sulfonamides which are prevalent in various biologically active compounds such as antimicrobial drugs and antitumor agents, enhance the toxicological pharmacological properties when combined with metal complexes; they can also be potentially used as radiopharmaceutical and imaging agents [30]. Sulfonamides are also present in numerous biologically active compounds such as antimicrobial drugs, saluretics, carbonic anhydrase inhibitors, insulin-releasing sulfonamides, antithyroid agents and antitumour drugs [31,32]. We ourselves noted in a previous study that sulfonamides show enhanced toxicological and pharmacological properties when combined with metals [33,34]. Thus, our objective has been to synthesize and characterize new rhenium sulfonamide metal complexes and evaluate their potential as serine/threonine kinase inhibitors using molecular docking studies.

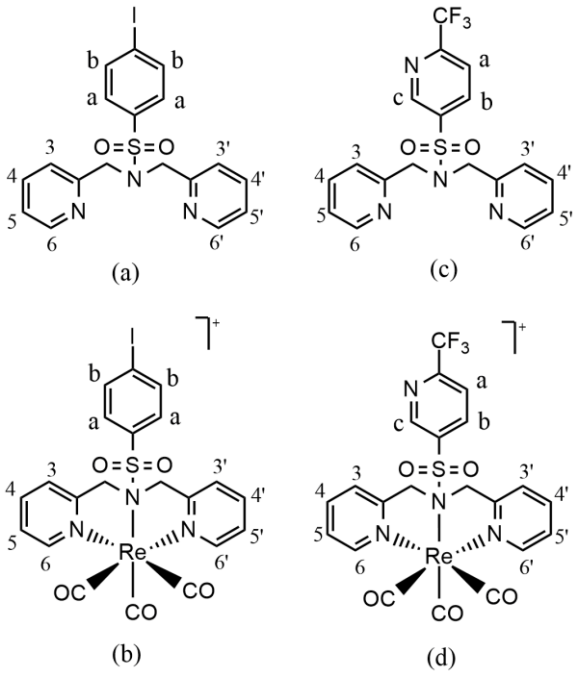

Fig. 1. Line diagram of a) $N(SO_2$(Iodobenz))dpa (**L1**), b) $[Re(CO)_3$**L1**$]^+$ (**C1**), c) $N(SO_2$(tfm)py)dpa (**L2**) and d) $[Re(CO)_3$**L2**$]^+$ (**C2**).

2. Results and Discussion

2.1 NMR spectroscopy

2.1.1 ^{1}H NMR spectroscopy

The **L1** ligand has previously been documented [35]; however, in this study, we achieved its synthesis with a notably higher yield through different synthetic approaches. Herein, we present ^{1}H NMR spectroscopic data in DMSO-d_6 alongside XRD spectroscopy data for **L1**. Peaks associated with residual solvent, including water and DMSO, were identified at 2.50

ppm and 3.33 ppm, respectively in its ^{1}H NMR spectra [36].

The signals corresponding to dipicolylamine were assigned based on previously reported data [37]. Protons H6/H6′, adjacent to the pyridyl nitrogen, were observed as the most downfield signals (8.35 ppm for **L1** and 8.28 ppm for **L2**), indicating their heightened deshielding in dipicolylamine. The signals for protons in the methylene groups of the ligands appeared as singlet peaks (4.54 ppm for **L1** and 4.66 ppm for **L2**). As reported in literature, these methylene group protons are magnetically equivalent due to free rotation, hence appearing as singlets in the NMR spectrum [8,38].

Conversely, the methylene protons in the complexes manifested as two doublets, shifted more downfield compared to the ligands (Fig. 2). Literature [8,38] suggests that upon coordination of the dipicolylamine ligand with the rhenium metal precursor, a new arrangement is attained for the methylene protons, rendering them magnetically nonequivalent. These protons are designated as *endo*-H and *exo*-H based on their orientation relative to the carbonyl, as previously described [8,38]. Comparison of NMR signals between the complex and the ligand revealed a downfield chemical shift (Fig. 2), attributable to the inductive effect exerted by rhenium upon direct bonding with N. The above findings serve as compelling evidence for metal complex formation.

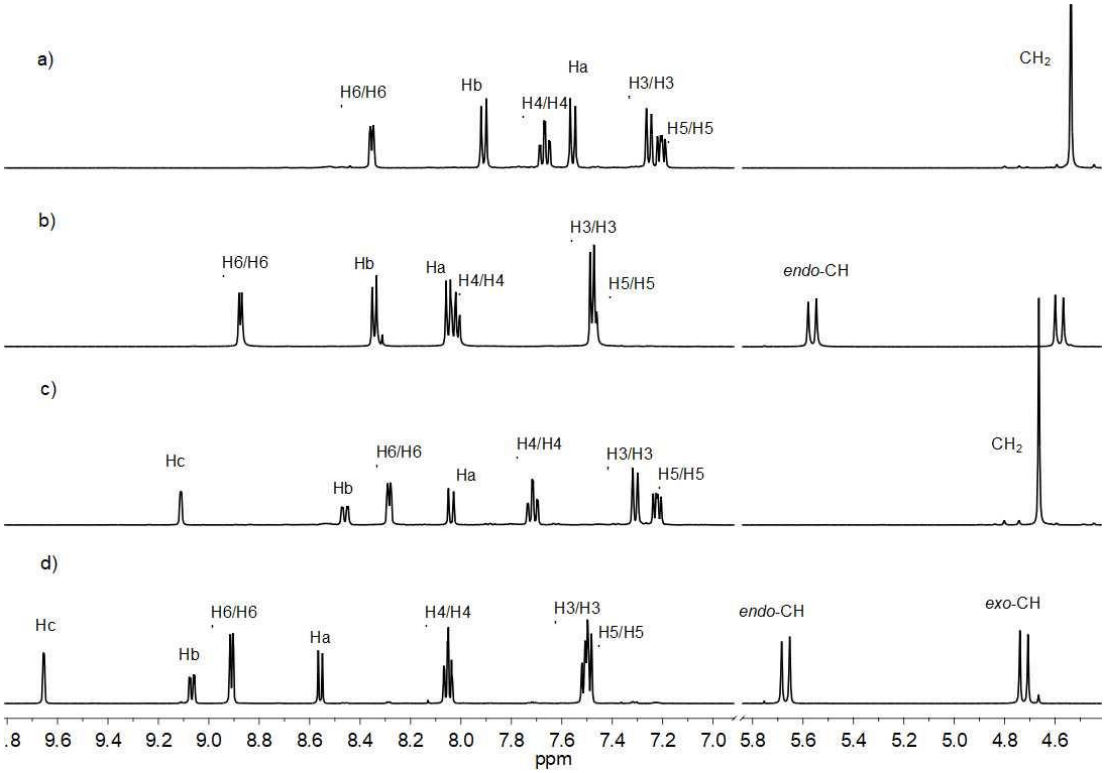

Fig. 2. ^{1}H NMR spectra of a) *N*(SO_2(Iodobenz))dpa (**L1**), b) [Re(CO)$_3$**L1**]$^+$ **(C1),** c) *N*(SO_2(tfm)py)dpa (**L2**) and d) [Re(CO)$_3$**L2**]$^+$ **(C2)** in DMSO-d_6.

2.1.2 ^{13}C NMR

Purity and the successful formation of the ligands and complexes were confirmed by ^{1}H NMR and ^{13}C NMR data. Upon complexation with the metal Re, pyridyl carbons of both ligands have shifted more downfield in the ^{13}C spectra of the two complexes (Fig. 3.). The signals in the range of 193 – 195 ppm attributed to the carbonyl groups ascertain that these are indeed terminal carbonyls of metal complexes, **C1** and **C2**.

a)

2.1.3 COSY and HSQC NMR

Further structural elucidation of the synthesized ligands; **L1** and **L2** were greatly aided by 2D NMR spectroscopy; COSY and HSQC (Fig. S.10, Fig. S.11, Fig. S.12 and Fig. S.13). ^{1}H correlations (3J ^{1}H-^{1}H couplings) were determined by the COSY spectra, and two distinct aromatic spin systems were identified for both **L1** and **L2** (Fig. 4. and Fig. 5.); i. DPA moiety and ii. Corresponding sulfonyl group (iodobenzene for **L1** and (tfm)py for **L2**). The sequential cross peaks show corresponding ^{1}H coupling patterns of the DPA moiety are clearly observed in the COSY spectra of both **L1** and **L2**. H5/5′ - H6/6′ (7.2 ppm and 8.3 ppm), H5/5′ - H4/4′ (7.2 ppm and 7.7 ppm), and H4/4′ - H3/3′ (7.7 ppm and 7.3 ppm) ensuring the DPA proton assignments. The COSY spectrum of **L1** shows ^{1}H coupling Ha-Hb (7.5 ppm and 7.9 ppm) while for **L2** the Ha-Hb coupling patterns are seen (8.0 ppm and 8.5 ppm). HSQC spectra (S.11 and Fig. S.13) were also taken into account to analyze the C-H correlations, and the spectra validate the structures of both **L1** and **L2** validating the ^{1}H assignments.

2.2 X-ray crystallographic data

Crystal data and details of the structural refinement for **L1**, **L2, C1** and **C2** are summarized in Table 1 and crystal structures of those compounds shown in Fig. 6 as ORTEPs drawn at 50% probability. The S-N bond of non-metal-coordinated sulfonamides are within the 1.62 Å - 1.64 Å range and also possess a near planar geometry around tertiary N [39,40]. The S-N bond of **L1**, 1.6366(15) Å and **L2,** 1.6205 (14) Å are within the above range. When considering the bond angles (Table 2) of *N*(SO_2(iodobenz))dpa and *N*(SO_2(tfm)py)dpa, the tertiary N atoms possess angles around 120°. The trigonal planar geometry around N for non-coordinate sulfonamide is indicated by 120° angle around N

which is sp^2 hybridized. The obtained values lie with the sp^2 hybridized N values as discussed here [40].

Tertiary sulfonamides bind to rhenium by rehybridization of sp^2 N to sp^3 N. According to literature the Re-N(sp^3) bond distance is within the range of 2.23-2.29 Å and Re-N(sp^2) within the range of 2.14-2.18 Å [37,38,41]. Similarly, structural data of **C1** and **C2** reveal Re1-N2 bonds of 2.259 Å and 2.288Å, respectively. Bond angles (Table 3) around the sulfonamide N are nearly equal to 109° and is another indication for sp^3 hybridization at the sulfonamide N [38]. According to the literature, trans angles of the rhenium complex are obtained in the range of 173.2°- 177.0° and show minor deviations from octahedral geometry [41]. Re-CO bond distances in the *fac*-$Re(CO)_3$ core are observed around 1.9 Å [41]. Structural results confirm that the complex bears a distorted octahedral geometry around the *fac*-$Re(CO)_3$ core.

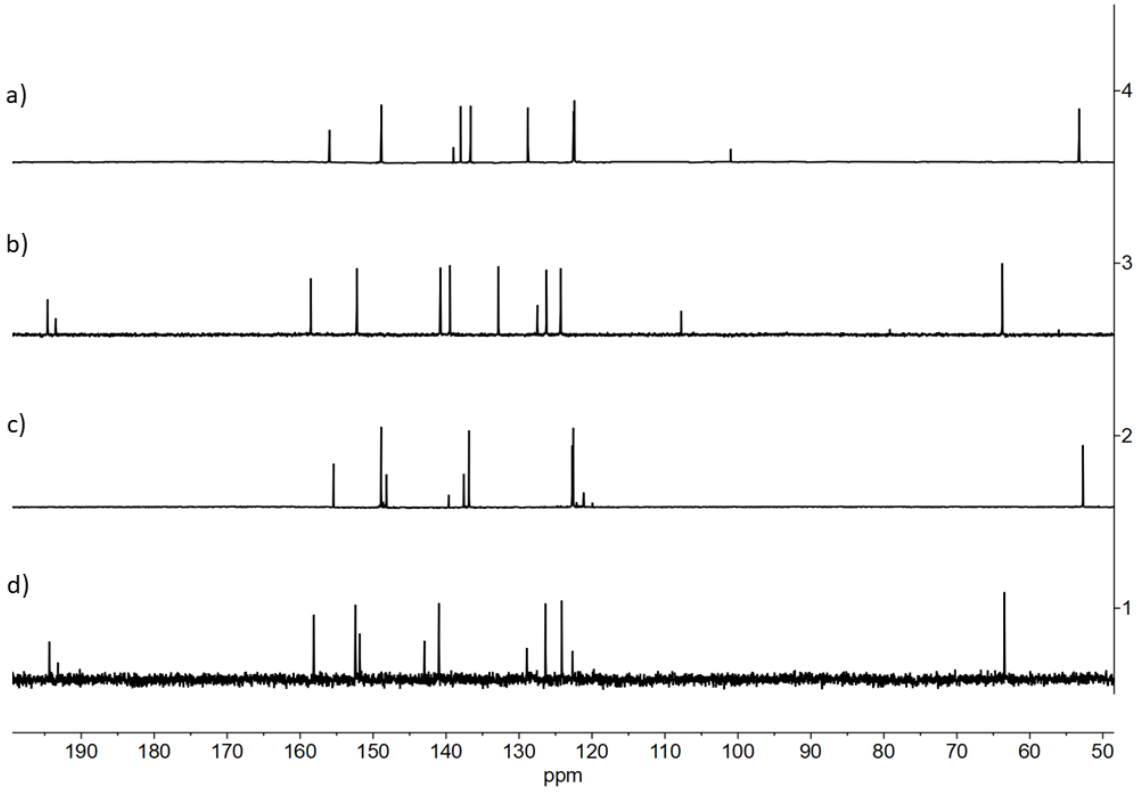

Fig. 3. ^{13}C NMR spectra of a) *N*(SO_2(Iodobenz))dpa (**L1**), b) [$Re(CO)_3$**L1**]$^+$ **(C1),** c) *N*(SO_2(tfm)py)dpa (**L2**) and d) [$Re(CO)_3$**L2**]$^+$ **(C2)** in DMSO-d_6.

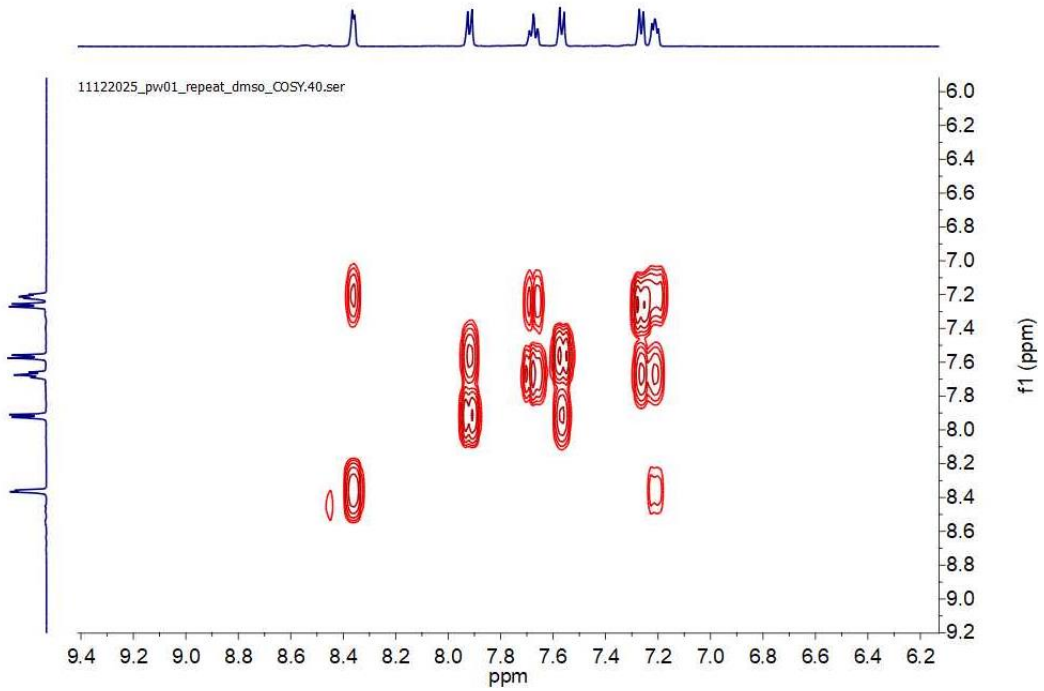

Fig. 4. COSY spectrum (aromatic region) of *N*(SO_2(Iodobenz))dpa (**L1**) in DMSO-d_6.

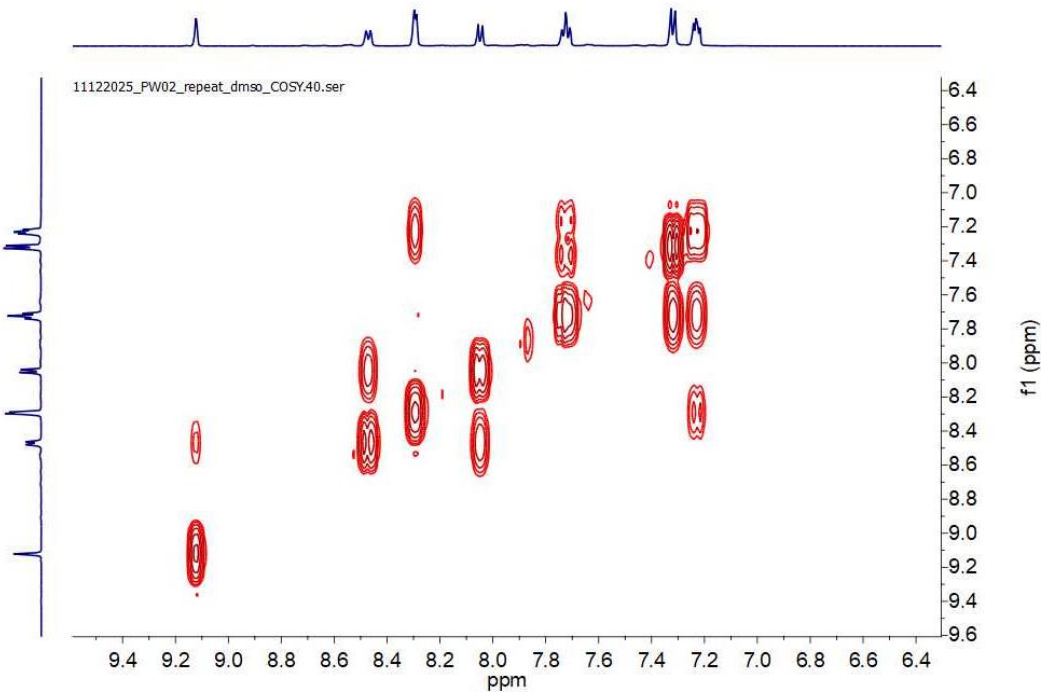

Fig. 5. COSY spectrum (aromatic region) of *N*(SO_2(tfm)py)dpa (**L2**) in DMSO-d_6.

Table 1. Crystal data and structure refinement of **L1**, **L2**, **C1** and **C2**.

Crystal data	L1	L2	C1	C2
Molecular formula	$C_{18}H_{16}IN_3O_2S$	$C_{18}H_{15}F_3N_4O_2S$	$C_{21}H_{16}IN_3O_5ReS\cdot 0.826(BF_4)\cdot 0.174(I)$	$C_{21}H_{15}F_3N_4O_5SRe.PF_6$
Mr	465.30	408.40	829.45	823.60
Crystal system	Triclinic	Monoclinic	Orthorhombic	Triclinic
Space group	*P* $\bar{1}$	*I2/a*	$P2_12_12_1$	*P* $\bar{1}$
Unit cell dimensions				
a (Å)	7.9629 (4)	23.3099 (13)	10.8624 (3)	12.8219 (4)
b (Å)	12.8004 (6)	6.1488 (4)	12.7681 (4)	15.3365 (5)
c (Å)	18.5913 (8)	26..524 (2)	18.1816 (5)	16.0045 (5)
α (deg)	95.211 (2)	_	-	103.6599 (18)
β (deg)	99.482 (2)	114.639 (3)	-	100.6477 (18)
γ (deg)	102.267 (2)	_	-	114.0384 (16)
V (Å^3)	1810.78 (15)	3455.5 (4)	2521.65 (13)	2649.25 (15)
T (K)	100	90	100	90
Z	4	8	4	4
D_x (Mgm^{-3})	1.707	1.570	2.184	2.065
abs coeff / μ (mm^{-1})	1.90	2.17	3.44	4.83
$2\theta_{max}$ (deg)	75.6 °	69.4 °	55.8 °	68.8 °
R[$F^2 > 2\sigma(F^2)$]	0.037	0.033	0.031	0.022
wR(F^2)	0.083	0.086	0.060	0.046
res. Dens (e Å^{-3})	-4.31 – 3.41	-0.45 – 0.48	-1.87 – 1.78	-0.94 – 1.15
Data/ parameters	19327/451	3171/253	12201/375	22261/757
Radiation type	Mo *Kα*	Cu *Kα*	Ag *Kα*	Mo *Kα*
Radiation wavelength/ λ (Å)	0.71073	1.54184	0.56086	0.71073

Table 2. Selected bond distances for **L1, L2, C1** and **C2**

Bond	Bond distance (Å)			
	L1	L2	C1	C2
S1—N2	1.6366 (15)	1.6205 (14)	1.757 (4)	1.7593 (15)
N1—C5	1.336 (2)	1.347 (2)	1.345 (6)	1.351 (2)
N1—C1	1.344 (3)	1.336 (2)	1.361 (6)	1.349 (2)
N3—C8	1.342 (2)	1.339 (2)	1.357 (6)	1.343 (2)
N3—C12	1.342 (2)	1.335 (2)	1.350 (6)	1.358 (2)
Re1—N3	-	-	2.178 (4)	2.1611 (15)
Re1—N1	-	-	2.174 (4)	2.1775 (16)
Re1—N2	-	-	2.259 (3)	2.2888 (14)
Re1—C19	-	-	1.928 (5)	1.927 (2)
Re1—C20	-	-	1.902 (5)	1.9048 (19)
Re1—C21	-	-	1.926 (5)	1.943 (2)

Table 3. Selected bond angles for **L1**, **L2**, **C1** and **C2**

Bond	Bond angle (°)			
	L1	**L2**	**C1**	**C2**
O2—S1—O1	119.53 (8)	120.66 (7)	121.3 (2)	121.47 (9)
O2—S1—N2	107.07 (8)	107.22 (7)	105.75 (19)	105.01 (8)
O1—S1—N2	106.47 (8)	106.90 (7)	104.1 (2)	105.38 (8)
O2—S1—C13	108.53 (8)	107.24 (7)	109.0 (2)	109.56 (8)
O1—S1—C13	107.83 (7)	106.96 (7)	110.9 (2)	108.10 (8)
C7—N2—C6	114.93 (15)	117.39 (13)	108.6 (3)	111.59 (13)
N2—C7—C8	111.70 (14)	111.70 (14)	108.8 (4)	114.36 (14)
C7—N2—S1	117.39 (12)	119.27 (11)	112.0 (3)	110.35 (11)
C6—N2—S1	116.09 (12)	118.75 (11)	111.0 (3)	108.59 (11)
C8—N3—C12	116.90 (15)	117.09 (15)	118.2 (4)	118.74 (16)
N2—C6—C5	112.39 (13)	113.98 (13)	113.0(3)	110.75 (14)
N3—Re1—N1	-	-	90.75 (14)	82.64 (6)
N3—Re1—N2	-	-	74.62 (13)	77.71 (5)
N1—Re1—N2	-	-	76.99 (13)	75.95 (5)
C7—N2—Re1	-	-	104.9 (3)	109.55 (10)
C6—N2—Re1	-	-	109.9 (2)	106.49 (10)
S1—N2—Re1	-	-	110.29(16)	110.21 (7)

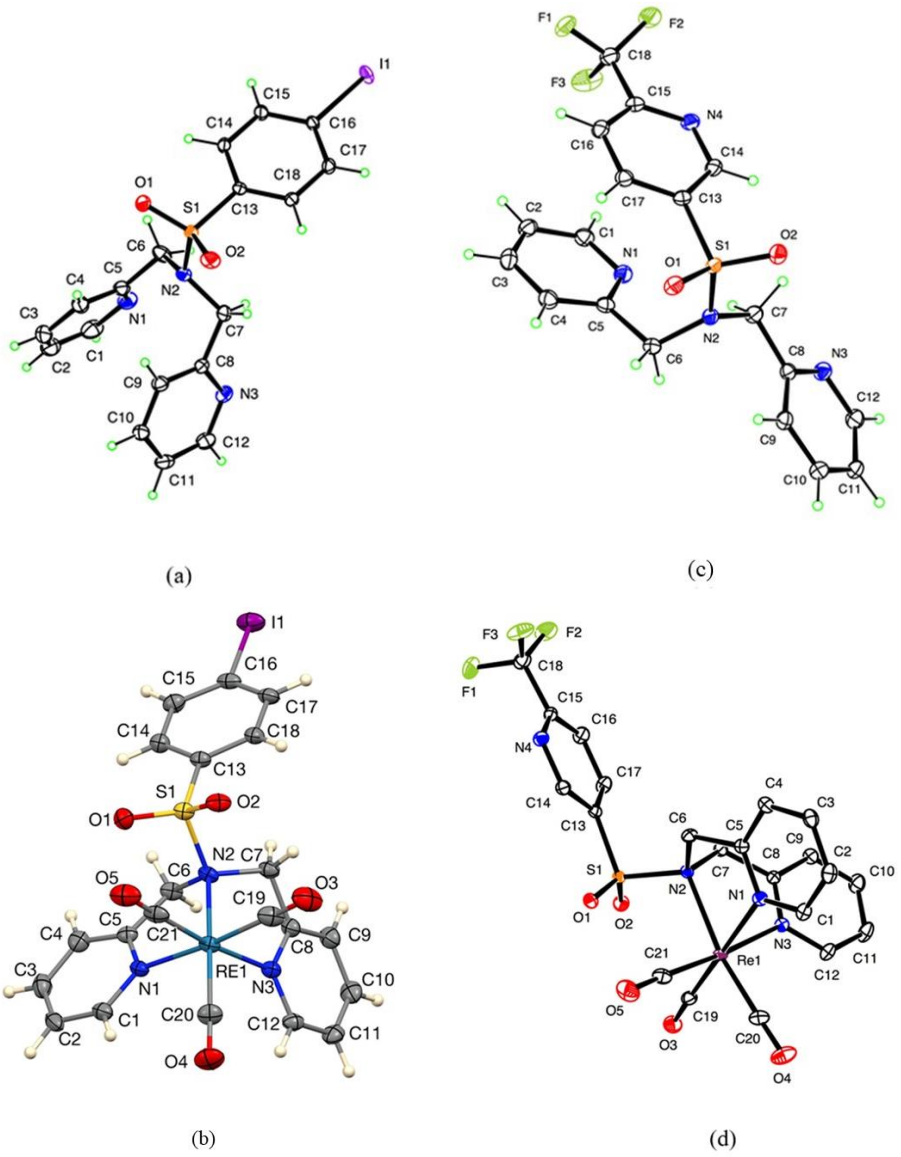

Fig. 6. ORTEP plots of a) *N*(SO_2(Iodobenz))dpa (**L1**), b) [$Re(CO)_3$**L1**]$^+$ (**C1**), c) *N*(SO_2(tfm)py)dpa (**L2** and d) [$Re(CO)_3$**L2**]$^+$ (**C2**). Thermal ellipsoids are drawn with 50% probability.

2.3 UV-Visible analysis

When considering the **L1** ligand and **C1** complex spectra in Fig. 7., **L1** displays peaks at 205 and 254 nm and **C1** displays a peak at 308 nm. As a result of π−π* transitions and the B band, 205 nm and 254 nm peaks may be present in the ligand. The peak near 308 nm in **C1** is due to a possible MLCT

transition. According to literature, MLCT transitions around 307 nm were assigned to $[Re(CO)_3(N(SO_2pip)dpa]^+$ [8], a complex which is comparable with **C1**. As shown in Fig. 7, **L2** ligand shows π−π* transitions including a B band, assigned at 206 and 261 nm whereas **C2** displays a MLCT around 307 nm [42, 43].

2.4 FTIR spectroscopy

Both complexes display characteristic IR peaks around 2039 and 1915 cm^{-1} (Fig. 8) due to the $Re(CO)_3$ core. However, the S-N stretching of **L1** ligand at 916 cm^{-1} has shifted to lower frequency in the $[Re(CO)_3\mathbf{L1}]BF_4$ complex (832 cm^{-1}) and S-N stretching of **L2** ligand (919 cm^{-1}) has also shifted to lower frequency in $[Re(CO)_3\mathbf{L2}]PF_6$ (830 cm^{-1}) in agreement with the general observation that lowering of the bond strength of S-N takes place upon binding to metal.

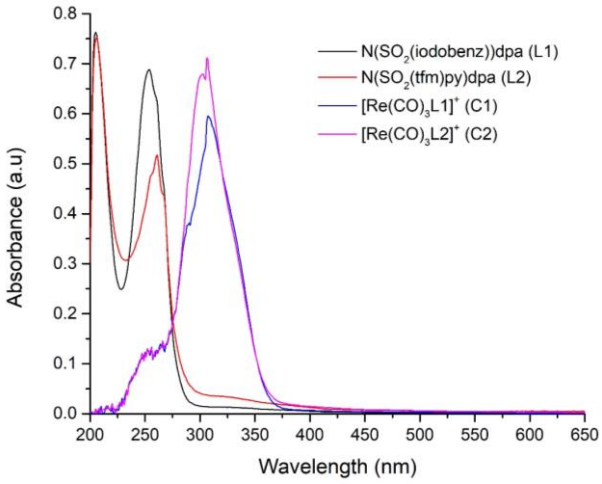

Fig. 7. UV-Visible spectra of $N(SO_2$(Iodobenz)dpa (**L1**), $N(SO_2$(tfm)dpa (**L2**), $[Re(CO)_3\mathbf{L1}]^+$ (**C1**) and $[Re(CO)_3\mathbf{L2}]^+$ (**C2**) in methanol at room temperature.

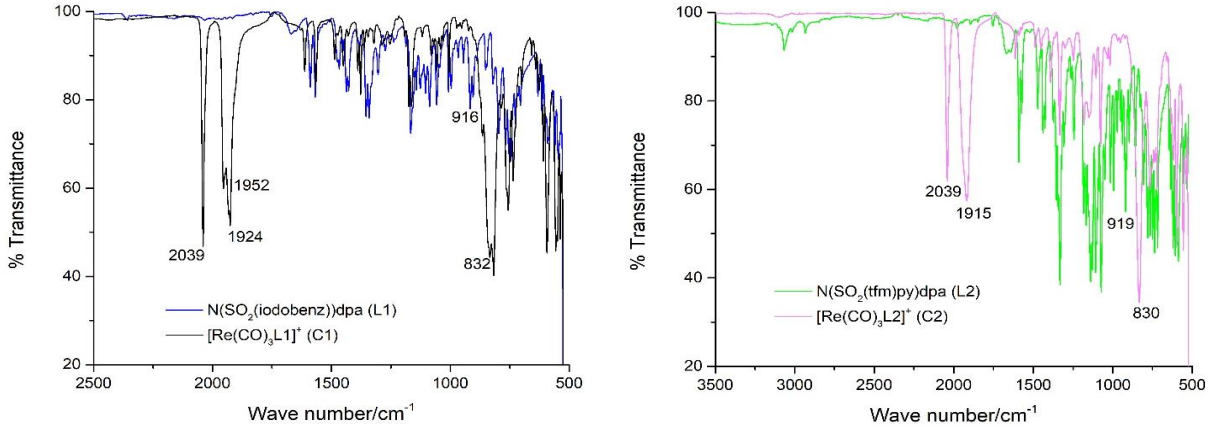

Fig. 8. FTIR spectra of $N(SO_2$(Iodobenz))dpa and $[Re(CO)_3\mathbf{L1}]^+$ (left) $N(SO_2$(tfm)py)dpa and $[Re(CO)_3\mathbf{L2}]^+$ (right).

2.5 Fluorescence data

L1 and **L2** ligands show fluorescence in methanol as shown in Table 4. However, the fluorescence intensities of both metal complexes have lowered possibly due to quenching occurred upon direct binding of sulfonamide nitrogen to metal (Fig. 9).

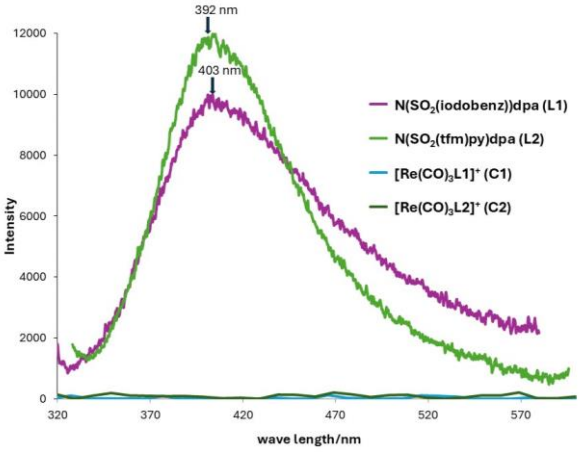

Fig. 9. Fluorescence spectra of $N(SO_2$(Iodobenz)dpa (**L1**), $N(SO_2$(tfm)py)dpa (**L2**), $[Re(CO)_3\mathbf{L1}]^+$ (**C1**) and $[Re(CO)_3\mathbf{L2}]^+$ (**C2**) in methanol at room temperature.

Table 4. Fluorescence data of **L1** and **L2** in methanol.

Compound	Excited wavelength/ nm	Emission wavelength/ nm
L1	300	403
L2	308	392

2.6 Target prediction and molecular docking results:

According to SwissTargetPrediction online tool, both ligands comply with the Lipinski rule of 5 [44–47]. Furthermore, **L1** is predicted to bind with serine/threonine protein kinase PIM2, while **L2** is predicted to bind with serine/threonine protein kinase Aurora-A. Currently, protein kinases are recognized as novel target for anticancer drug development [48]. Docking has been carried out by using Molegro Virtual Docker 2014.6.0.1 software. **L1** and **C1** were docked with the PIM2 kinase protein (PDB ID: 4X7Q) and **L2** and **C2** were docked with Aurora-A kinase protein (PDB ID: 1MQ4). MolDock score for ligands and complexes are shown in Table 5.

Table 5. MolDock score data of ligands and complexes.

Compound	MolDock score
L1	-115.98
C1	-140.668
L2	-114.376
C2	-134.5

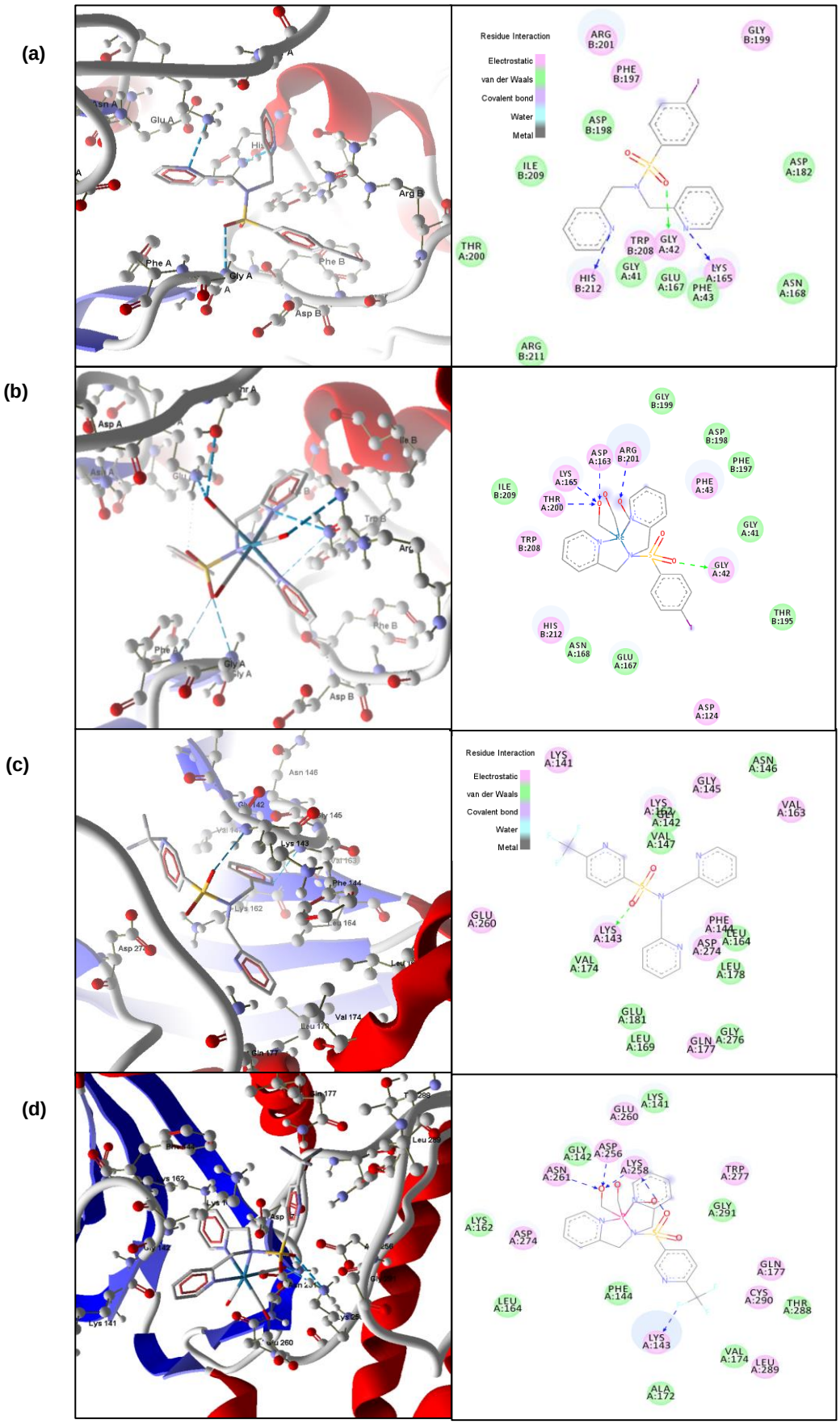

Fig. 10. Docking results and amino acid interactions a) **L1**, b) **C1**, c) **L2** and d) **C2.**

The MolDock scoring function is based on a modified piecewise linear potential (PLP) that calculates the ligand-protein binding energy. An overall docking score is produced by combining terms that account for steric, hydrogen bonding,

and electrostatic interactions. In the active site, a ligand with a lower MolDock score usually has a more advantageous and stable binding conformation. The binding affinities of various ligands to the target protein can thus be ranked and compared with the aid of this scoring system [49,50].

L1 has H-bonding with Lys 165(A) and His 212(B) amino acids and steric interaction with Gly 42(A) while **C1** has H-bonding with Thr 200(A), Arg 201(B), Asp 163(A) and Lys 165(A), amino acids and steric interaction with Gly 42(A). **L2** is bonding through steric interactions with Lys 143(A) and **C2** have H-bonding with Asn 261(A), Asp 256(A), Lys 258(A) and Lys 143(A). The active sites of PIM2 kinase protein and Aurora-A kinase are ASP 163(A) (**https://www.rcsb.org/sequence/4X7Q#A**) and ASP 137(A) (**https://www.rcsb.org/sequence/1MQ4#A**), respectively. According to these results, only the interactions of **C1** occur within the active site of the protein, while the interactions of **L1**, **L2** and **C2** occur near the active site of the protein. The final docking structures and interactions with amino acids are shown in Fig. 10. Therefore, it can be concluded that the **C1** complex is the most effective compared to the other compounds, as it interacts directly within the active site of the protein and achieves the lowest MolDock score. The molecular docking results underscore the potential binding affinities of the synthesized compounds; **L1**, **L2**, **C1** and **C2** with serine/threonine protein kinases, indicating their potential to be developed as anticancer drug leads.

3. Material and Methods

3.1 Materials and methods; Di-(2-picolyl)amine (DPA), 6-(trifluoromethyl)pyridine-3-sulfonyl chloride, 4-iodobenzenesulfonyl chloride, $Re_2(CO)_{10}$, AgOTf, $NaPF_6$, $NaBF_4$, dichloromethane, chromasolv water, dioxane, acetone and methanol were used as received from Sigma Aldrich.

3.2 NMR analysis: ^{1}H NMR, ^{13}C NMR, COSY and HSQC spectra were recorded in DMSO-d_6 using a Bruker 400 MHz and 125 MHz spectrometer, respectively. Peak positions are relative to DMSO-d_6 or solvent residual peak, with trimethylsilane (TMS) as reference. NMR data were processed with MestReNova software.

3.3 X-ray data Collection and structure determination; Diffraction data were collected at low temperature with Bruker *APEX-II* DUO CCD and Bruker D8 Venture diffractometers. Radiation sources were Mo $K\alpha$ (λ= 0.71073 Å) radiation for **L1** and $[Re(CO)_3$**L2**$]PF_6$, Cu $K\alpha$ (λ= 1.54184 Å) for **L2** and Ag Kα for $[Re(CO)_3$**L1**$]BF_4$. Data were collected for **L1** and $[Re(CO)_3$**L1**$]BF_4$ at 100 K and for **L2** and $[Re(CO)_3$**L2**$]PF_6$ at 90 K. Data reduction done with Bruker *SAINT* and includes absorption correction using multi-scan on *SADABS*. In the structure of $[Re(CO)_3$**L1**$]BF_4$, the anion is partially occupied (17.4%) by iodide. Molecular graphics are drawn using ORTEP-3 for windows and Mercury. The structural data have been deposited with the Cambridge Crystallographic Data Centre under deposition numbers CCDC 2431548-2431551.

3.4 FTIR analysis; Thermo Scientific Nicolet iS10 FTIR spectrometer was used. ATR spectra were processed within the 4000-500 cm^{-1} spectral range by OMINIC Spectra™ software.

3.5 UV-Visible spectroscopy: Spectra were recorded for synthesized ligands and complexes by using Thermo Scientific GENESYS™ 10S series UV-VIS spectrophotometer. The spectral range was 190 nm to 1100 nm. All the spectra recorded in methanol with baseline correction with the aid of VISIONlite™ software.

3.6 Fluorescence data analysis: Emission spectra of the ligands were obtained in methanol on Thermo Scientific Lumina Fluorescence spectrometer. Excitation source was 150 W Xenon lamp. Luminous software was used to process spectra.

3.7 Synthesis: In order to synthesize rhenium complexes, $[Re(CO)_3(H_2O)_3]OTf$ metal precursor was synthesized by a known method [11].

3.7.1. *N*(SO_2(Iodobenz))dpa **(L1)** synthesis; A solution of 4-iodobenzenesulfonyl chloride, (0.796 g, 2.5 mmol) in 12.5 mL of dioxane was added dropwise over a period of 2 h to a solution of DPA (0.928 mL, 5 mmol) in 50 mL of dioxane at 20 °C. The reaction mixture was stirred at room temperature for 24 h and then filtered to remove any precipitate before the dioxane was completely removed by rotary evaporation. Chromasolv water 30 mL (pH~ 5) was added to the resulting solid and the product was extracted into dichloromethane (2 x 25 mL). The dichloromethane extracts were combined, washed with chromasolv water (2 x 25 mL), and the solvent was evaporated to yield brownish orange colour, block like crystals (0.768 g, 66% yield). Single crystals suitable for X-ray diffraction were obtained by slow evaporation of methanol. ^{1}H NMR signals (ppm) in DMSO-d_6; 8.35(d, 2H, H6/H6′), 7.91 (d, 2H, Hb), 7.67 (t, 2H, H4/H4′), 7.56 (d, 2H, Ha), 7.25 (d, 2H, H3/H3′). 7.21(t, 2H, H5/H5′) and 4.54 (s, 4H, CH_2). ^{13}C NMR signals (ppm) in DMSO-d_6; 148.74 (C6/C6′), 137.34 (Cb), 136.81 (C4/C4′), 128.43 (Ca), 122.28 (C3/C3′ and C5/C5′), 53.25 (CH_2).

3.7.2 *N*(SO_2(tfm)py)dpa **(L2)** synthesis; A solution of 6-trifluoromethylpyridine-3-sulfonyl chloride (0.633 g, 2.5 mmol) in 12.5 mL of dioxane was added dropwise over a period of 2 h to a solution of DPA (0.928 mL, 5 mmol) in 50 mL of dioxane at 20 °C. The reaction mixture was stirred at room temperature for 24 h and then filtered to remove any precipitate before the dioxane was completely removed by rotary evaporation. Chromasolv Water 30 mL (pH~5) was added to the resulting solid and the product was extracted into dichloromethane (2 x 25 mL). The dichloromethane extracts were combined, washed with chromasolv water (2 x 25 mL), and the solvent was evaporated to yield light orange color, thread like crystals (0.990 g, 97% yield). Single crystals suitable for X-ray diffraction were obtained by slow evaporation of acetone. ^{1}H NMR signals (ppm) in DMSO-d_6; 9.11 (s, 1H, Hc), 8.46 (d, 1H, Hb), 8.28(d, 2H, H6/H6′), 8.03 (d, 1H, Ha), 7.71 (t, 2H, H4/H4′), 7.30 (d, 2H, H3/H3′). 7.22 (t, 2H, H5/H5′) and 4.66 (s, 4H, $2CH_2$). ^{13}C NMR signals (ppm) in DMSO-d_6; 148.74 (C6/C6′), 148.08 (Cc), 137.31 (Ca), 136.5 (C4/C4′), 139.56 (Cb), 122.58 (C3/C3′ and C5/C5′), 52.65 (CH_2).

3.7.3 $[Re(CO)_3(N(SO_2$(Iodobenz))dpa$)]^+$ (**C1**) synthesis; A solution of N(SO_2(Iodobenz))dpa (0.047 g, 0.1 mmol) in 2.00

mL water and 5.00 mL methanol was treated with aqueous $[Re(CO)_3(H_2O)_3]OTf$ (1.00 mL, 0.1 mmol). The acidity of the solution was measured (pH~5). After that the clear solution was heated at reflux overnight. A slight excess of $NaBF_4$ was added to the clear solution and resultant precipitate was filtered. Then the precipitate was allowed to dry (0.037 g, 44% yield). Single crystals suitable for X-ray diffraction were obtained by slow evaporation of methanol. ^{1}H NMR signals (ppm) in DMSO-d_6; 8.87 (d, 2H, H6/H6′), 8.35 (d, 2H, Hb), 8.05 (d, 2H, Ha), 8.02 (t, 2H, H4/H4′), 7.49-7.46 (m, 4H, H3/H3′ and H5/H5′), 5.56 (d, 2H, *endo*-H) and 4.58 (d, 2H, *exo*-H). ^{13}C NMR signals (ppm) in DMSO-d_6; 193.51, 194.61 (CO), 152.09 (C6/C6′), 140.47 (C4/C4′), 140.45 (Cb), 132.79 (Ca), 127.42 (C3/C3′), 124.29 (C5/C5′), 63.76 (CH_2).

3.7.4 $[Re(CO)_3(N(SO_2(tfm)py)dpa)]^+$ (**C2**) synthesis; A solution of $N(SO_2(tfm)py)dpa$ (0.041 g, 0.1 mmol) in 2.00 mL water and 5.00 mL methanol was treated with aqueous $[Re(CO)_3(H_2O)_3]OTf$ (1.00 mL, 0.1 mmol). The acidity of the solution was measured (pH~5). After that the clear solution was heated at reflux overnight. A slight excess of $NaPF_6$ was added to the clear solution and resultant precipitate was filtered. Then the precipitate was allowed to dry (0.030 g, 38% yield). Single crystals suitable for X-ray diffraction were obtained by slow evaporation of methanol. ^{1}H NMR signals (ppm) in DMSO-d_6; 9.65 (s, 1H, Hc), 9.07 (d, 1H, Hb), 8.90 (d, 2H, H6/H6′), 8.56 (d, 1H, Ha), 8.05 (t, 2H, H4/H4′), 7.50 (m, 4H, H3/H3′ and H5/H5′), 5.67 (d, 2H, *endo*-H) and 4.72 (d, 2H, *exo*-H). ^{13}C NMR signals (ppm) in DMSO-d_6; 193.20, 194.38 (CO), 151.87 (C6/C6′), 152.01 (Cc), 140.21 (Ca), 140.76 (C4/C4′), 142.41 (Cb), 126.00 (C3/C3′), 123.39 (C5/C5′), 63.00 (CH_2).

3.8 Target prediction and molecular docking: Probable macromolecular targets for the ligands and their complexes were predicted using SwissTargetPrediction web tool [51, 52]. Protein structure of Serine Threonine protein kinase (PDB ID: 4X7Q for **L1** and **C1** and 1MQ4 for **L2** and **C2**) was prepared by deleting bound ligands, water and adding polar H atoms using Chimera 1.9 software [53]. The .cif files of ligands and complexes obtained from single crystal X-ray data were converted to PDB format using Avogadro 1.0.1 software. Blind docking was carried out using Molegro Virtual Docker 2014.6.0.1 software. The complex with the lowest binding energy was taken and ligand interactions were visualized with the same software.

4. Conclusions

We have successfully synthesized and characterized novel rhenium complexes with potential as kinase inhibitors, opening avenues for new cancer therapies. Spectroscopic analysis via NMR spectroscopy, UV-Visible spectroscopy, and FTIR spectroscopy techniques corroborate the formation of these complexes, with notable shifts in spectral peaks providing evidence of successful ligand integration. X-ray crystallography confirmed the anticipated structures and bond rehybridizations, which align with similar compounds reported in literature. Fluorescence studies revealed quenching effects post-complexation, indicative of altered electronic environments. The potential of these complexes to act as kinase inhibitors was substantiated through computational predictions and molecular docking studies, which illustrated a high likelihood of interaction with key protein kinases involved in cancer proliferation. This suggests a robust starting point for the creation of new therapeutic agents. Future research, focused on *in vivo* studies and clinical trials, will be crucial in determining the practical applicability of these findings in medical treatments.

Supporting Information

Available.

Acknowledgments

The authors would like to acknowledge the Instrument Center, Faculty of Applied Sciences, University of Sri Jayewardenepura, Sri Lanka for supporting with the instrumentation and Auburn University NMR Facilities Center and Dr. Ethan Hill for their valuable support and provision of the 2D NMR data. Financial Assistance by the university research grant; ASP/01/RE/SCI/2021/17.

Author Contributions

Pamodya P Weerasuriya, Kithmini Yasarathna, Lashan Edirisinghe: Investigation, Formal analysis, Methodology, Writing - original draft. Frank R. Fronczek: Investigation, Resources, Formal analysis, Data curation. Inoka C Perera: Investigation, Resources, Formal analysis, Data curation. Theshini Perera: Methodology, Conceptualization, Supervision, Writing - review & edit.

References and Notes

[1] Adhikari, S.; Nath, P.; Das, A.; Datta, A.; Baildya, N.; Duttaroy, A. K. et al. *Biomed. Pharmacother.* **2024**, *171*, 116211. [Crossref]

[2] Köpf-Maier, P. *Eur. J. Clin. Pharmacol.* **1994**, *47*, 1. [Crossref]

[3] Casini, A.; Pöthig, A. *ACS Cent. Sci.* **2024**, *10*, 242. [Crossref]

[4] Muhammad, N.; Hanif, M.; Yang, P. *Coord. Chem. Rev.* **2024**, *499*, 215507. [Crossref]

[5] Che, C. M.; Siu, F. M. *Curr. Opin. Chem. Biol.* **2010**, *14*, 255. [Crossref]

[6] Abdolmaleki, S.; Aliabadi, A.; Khaksar, S. *Coord. Chem. Rev.* **2024**, *501*, 215579. [Crossref]

[7] Marker, S. C.; King, A. P.; Granja, S.; Vaughn, B.; Woods, J. J.; Boros, E.; Wilson, J. J. *Inorg. Chem.* **2020**, *59*, 10285. [Crossref]

[8] Subasinghe, A.; Perera, I. C.; Pakhomova, S.; Perera, T. *Bioinorg. Chem. Appl.* **2016,** 2675937. [Crossref]

[9] Leonidova, A.; Gasser, G. *ACS Chem. Biol.* **2014**, *9*, 2180. [Crossref]

[10] Storr, T.; Thompson, K. H.; Orvig, C. *Chem. Soc. Rev.* **2006**, *35*, 534. [Crossref]

[11] He, H.; Lipowska, M.; Xu, X.; Taylor, A. T.; Carlone, M.; Marzilli, L. G. *Inorg. Chem.* **2005**, *44*, 5437. [Crossref]

[12] Hostachy, S.; Policar, C.; Delsuc, N. *Coord. Chem. Rev.* **2017**, *351*, 172. [Crossref]

[13] Schibli, R.; Netter, M.; Scapozza, L.; Birringer, M.; Schelling, P.; Dumas, C. et al. *J. Organomet. Chem.* **2003**, *668*, 67. [Crossref]

[14] Pollard, J. R.; Mortimore, M. *J. Med. Chem.* **2009**, *52*, 2629. [Crossref]

[15] Asati, V.; Mahapatra, D. K.; Bharti, S. K. *Eur. J. Med. Chem.* **2019**, *172,* 95. [Crossref]

[16] Atalay, P.; Ozpolat, B. *Cancers* **2024**, *16*, 535. [Crossref]

[17] Panchal, N. K.; Sabina, E. P. *Life Sci.* **2020**, *255*, 117866. [Crossref]

[18] Keen, N.; Taylor, S. *Nat. Rev. Cancer* **2004**, *4*, 927. [Crossref]

[19] Katayama, H.; Sen, S. *Biochim. Biophys. Acta, Gene Regul. Mech.* **2010**, *1799,* 829. [Crossref]

[20] Guo, T.; Ma, S. *ChemMedChem* **2021**, *16*, 600. [Crossref]

[21] De, S.; Nag, S. *Rev. Inorg. Chem.* **2024**, *44*, 1. [Crossref]

[22] Hartinger, C. G.; Metzler-Nolte, N.; Dyson, P. J. *Organometallics* **2012,** *31*, 5677. [Crossref]

[23] Steel, T. R.; Walsh, F.; Wieczorek-Błauż, A.; Hanif, M.; Hartinger, C. G. *Coord. Chem. Rev.* **2021**, *439*, 213890. [Crossref]

[24] Mertens, R. T.; Gukathasan, S.; Arojojoye, A. S.; Olelewe, C.; Awuah, S. G. *Chem. Rev.* **2023**, *123*, 6612. [Crossref]

[25] Domenichini, A.; Casari, I.; Simpson, P. V.; Desai, N. M.; Chen, L.; Dustin, C. et al. *J. Exp. Clin. Cancer Res.* **2020**, *39*, 276. [Crossref]

[26] Simpson, P. V.; Casari, I.; Paternoster, S.; Skelton, B. W.; Falasca, M.; Massi, M. *Chem. - Eur. J.* **2017**, *23*, 6518. [Crossref]

[27] Torres Martin de Rosales, R.; Finucane, C.; Foster, J.; Mather, S. J.; Blower, P. J. *Bioconjugate Chem*. **2010**, *21*, 811. [Crossref]

[28] Storr, T.; Fisher, C. L.; Mikata, Y.; Yano, S.; Adam, M. J.; Orvig, C. *Dalton Trans.* **2005**, *4*, 654. [Crossref]

[29] Storr, T.; Sugai, Y.; Barta, C. A.; Mikata, Y.; Adam, M. J.; Yano, S. et al. *Inorg. Chem.* **2005**, *44*, 2698. [Crossref]

[30] Dilworth, J. R.; Pascu, S. I.; Waghorn, P. A.; Vullo, D.; Bayly, S. R.; Christlieb, M. et al. *Dalton Trans.* **2015**, *44*, 4859. [Crossref]

[31] Abou El Ella, D. A.; Ghorab, M. M.; Heiba, H. I.; Soliman, A. M. *Med. Chem. Res.* **2012**, *21*, 2395. [Crossref]

[32] Özbek, N.; Katırcıoğlu, H.; Karacan, N.; Baykal, T. *Bioorg. Med. Chem.* **2007**, *15*, 5105. [Crossref]

[33] Chohan, Z. H. *J. Enzyme Inhib. Med. Chem.* **2008**, *23*, 120. [Crossref]

[34] Chohan, Z. H.; Youssoufi, M. H.; Jarrahpour, A.; Hadda, T. B. *Eur. J. Med. Chem.* **2010**, *45*, 1189. [Crossref]

[35] He, X.; Zhu, N.; Yam, V. W. W. *Organometallics* **2009**, *28*, 3621. [Crossref]

[36] Silverstein, R. M.; Bassler, G. C. *J. Chem. Educ.* **1962**, *39*, 546. [Crossref]

[37] Perera, T.; Abhayawardhana, P.; Marzilli, P. A.; Fronczek, F. R.; Marzilli, L. G. *Inorg. Chem.* **2013**, *52*, 2412. [Crossref]

[38] Ranasinghe, K.; Marzilli, P. A.; Pakhomova, S.; Marzilli, L. G. *Inorg. Chim. Acta* **2022**, *533*, 120781. [Crossref]

[39] Veltzé, S.; Egdal, R. K.; Johansson, F. B.; Bond, A. D.; McKenzie, C. J. *Dalton Trans.* **2009**, *47*, 10495. [Crossref]

[40] Darshani, T.; Thushara, N.; Weerasuriya, P.; Fronczek, F. R.; Perera, I. C.; Perera, T. *Polyhedron* **2020**, *185*, 114592. [Crossref]

[41] Banerjee, S. R.; Levadala, M. K.; Lazarova, N.; Wei, L.; Valliant, J. F.; Stephenson, K. A. et al. *Inorg. Chem.* **2002**, *41*, 6417. [Crossref]

[42] Rohacova, J.; Ishitani, O. *Dalton Trans.* **2017**, *46*, 8899. [Crossref]

[43] Fernández-Moreira, V.; Marzo, I.; Gimeno, M. C. *Chem. Sci.* **2014**, *5*, 4434. [Crossref]

[44] Lipinski, C. A.; Lombardo, F.; Dominy, B. W.; Feeney, P. J. *Adv. Drug Delivery Rev.* **1997**, *23*, 3. [Crossref]

[45] Chagas, C. M.; Moss, S.; Alisaraie, L. *Int. J. Pharm.* **2018**, *549*, 133. [Crossref]

[46] Chen, X.; Li, H.; Tian, L.; Li, Q.; Luo, J.; Zhang, Y. *J. Comput. Biol.* **2020**, *27*, 397. [Crossref]

[47] Veber, D. F.; Johnson, S. R.; Cheng, H. Y.; Smith, B. R.; Ward, K. W.; Kopple, K. D. *J. Med. Chem.* **2002**, *45*, 2615. [Crossref]

[48] Singh, H.; Kumar, R.; Mazumder, A. *J. Asian Nat. Prod. Res.* **2024**, *26*, 663. [Crossref]

[49] Thomsen, R.; Christensen, M. H. *J. Med. Chem.* **2006**, *49*, 3315. [Crossref]

[50] Kaluthanthiri, D.; Rajagopalan, U.; Fronczek, F. R.; Samarakoon, S.; Weerasinghe, L.; Perera, I. C. et al. *Polyhedron* **2024**, *255*, 117131. [Crossref]

[51] Daina, A.; Michielin, O.; Zoete, V. *Nucleic Acids Res.* **2019**, *47*, W357. [Crossref]

[52] Gfeller, D.; Michielin, O.; Zoete, V. *Bioinformatics* **2013**, *29*, 3073. [Crossref]

[53] Pettersen, E. F.; Goddard, T. D.; Huang, C. C.; Couch, G. S.; Greenblatt, D. M.; Meng, E. C. et al. *J. Comput. Chem.* **2004,** *25*, 1605. [Crossref]

How to cite this article

Weerasuriya P. P.; Yasarathna, K.; Edirisinghe, L.; Fronczek, F. R.; Perera, I. C.; Perera, T. *Orbital: Electronic J. Chem*. **2025**, *17*, 540. DOI: http://dx.doi.org/10.17807/orbital.v17i6.23219